Science Bulletin 70 (2025) 756–764

Contents lists available at ScienceDirect

Science Bulletin

journal homepage: www.elsevier.com/locate/scib

Article

Transition from multi-year La Niña to strong El Niño rare but increased under global warming

Fan Jia [a,b,*], Wenju Cai [b,c,d,e,*], Tao Geng [b], Bolan Gan [c], Wenxiu Zhong [f], Lixin Wu [b,c], Michael J. McPhaden [g]

[a] Key Laboratory of Ocean Observation and Forecasting and Key Laboratory of Ocean Circulation and Waves, Institute of Oceanology, Chinese Academy of Sciences, Qingdao 266000, China
[b] Laoshan Laboratory, Qingdao 266237, China
[c] Frontier Science Center for Deep Ocean Multispheres and Earth System (FDOMES) and Physical Oceanography Laboratory, Ocean University of China, Qingdao 266100, China
[d] State Key Laboratory of Loess and Quaternary Geology, Institute of Earth Environment, Chinese Academy of Sciences, Xi'an 710061, China
[e] State Key Laboratory of Marine Environmental Science & College of Ocean and Earth Sciences, Xiamen University, Xiamen 361005, China
[f] School of Atmospheric Sciences, Sun Yat-sen University, Southern Marine Science and Engineering Guangdong Laboratory (Zhuhai), Zhuhai 519000, China
[g] NOAA/Pacific Marine Environmental Laboratory, Seattle, Washington DC 20005, USA

ARTICLE INFO

Article history:
Received 12 August 2024
Received in revised form 28 November 2024
Accepted 29 November 2024
Available online 25 December 2024

Keywords:
El Niño-Southern Oscillation transition
multiyear La Niña
greenhouse warming
atmosphere deep convection

ABSTRACT

El Niño-Southern Oscillation (ENSO) exhibits a strong asymmetry between warm El Niño and cold La Niña in amplitude and temporal evolution. An El Niño often leads to a heat discharge in the equatorial Pacific conducive to its rapid termination and transition to a La Niña, whereas a La Niña persists and recharges the equatorial Pacific for consecutive years preconditioning development of a subsequent El Niño, as occurred in 2020–2023. Whether the multiyear-long heat recharge increases the likelihood of a transition to a strong El Niño remains unknown. Here, we show that such a transition is rare but more likely under transient greenhouse warming. In boreal spring and early summer after a multiyear La Niña, despite a substantial recharge in the western Pacific, thermocline remains anomalously shallow and sea surface temperature (SST) remains anomalously cold in the equatorial central Pacific. The cold conditions inhibit an ensuing eastward movement of atmosphere deep convection out of the warm western Pacific, delaying onset of ocean-atmosphere coupling, and hence growth of an El Niño. Under a high emission scenario, such a transition is still rare but more than twice as likely. The projected change is consistent with a projected weakening in climatological zonal SST gradient that promotes the eastward movement of atmosphere convection and a projected intensification in upper-ocean stratification of the equatorial Pacific that enhances the ocean-atmosphere coupling. Our result provides predictive insight of El Niño after multiyear La Niña, and advances our understanding of ENSO transition under greenhouse warming.
© 2024 The Authors. Published by Elsevier B.V. and Science China Press. This is an open access article under the CC BY license (http://creativecommons.org/licenses/by/4.0/).

1. Introduction

El Niño-Southern Oscillation (ENSO), varying irregularly between its warm phase El Niño and cold phase La Niña, is the most energetic year-to-year climate variation on Earth and has highly consequential impacts on global extreme weather, ecosystem and economy [1–4]. During boreal spring when an El Niño develops, a relaxation of trade winds triggers downwelling equatorial Kelvin waves, creating a flattened equatorial Pacific thermocline, a reduced upwelling in the eastern Pacific and a surface warming in the central and eastern Pacific. The atmosphere convection center moves eastward following the warm SST, which further weakens the trade winds to the west of the convection, in turn intensifying the surface warming in a positive Bjerknes feedback [5]. The eastward shift in convection is crucial for the growth of El Niño and its remote influence [6–11]. The deep convection usually reaches the Date Line during a moderate El Niño, but extends to the eastern Pacific during a strong and extreme El Niño. Such strong shifts bring intense rainfall to the normally cold and dry eastern equatorial Pacific region, generating atmospheric teleconnections that severely disrupt global climate [7,10–13].

El Niño wind anomalies discharge heat out of the equatorial Pacific [14]. In boreal winter, the westerly wind anomalies shift southward out of the equator due to a southward migration of the western Pacific warm pool and an intensification of the South Pacific convergence zone [15,16]. These anomalies, together with the discharged equatorial upper ocean heat content and the seasonally weakened ocean-atmosphere coupling, lead to a rapid termination of El Niño. During La Niña, the reverse occurs but with an

* Corresponding authors.
E-mail addresses: fjia@qnlm.ac (F. Jia), cwjresearch@gmail.com (W. Cai).

https://doi.org/10.1016/j.scib.2024.12.034
2095-9273/© 2024 The Authors. Published by Elsevier B.V. and Science China Press.
This is an open access article under the CC BY license (http://creativecommons.org/licenses/by/4.0/).

asymmetric spatial pattern, amplitude and temporal evolution [17–20]; the associated wind anomalies recharge the equatorial Pacific for development of a subsequent El Niño. Warm SST anomalies of El Niño develop and mature within one year, and are stronger in amplitude and more eastward in anomaly center than cold SST anomalies of La Niña. A La Niña often follows an El Niño and lasts for multiple years [21–25], as in 2020–2022, when a three-year La Niña occurred, causing prolonged and aggregated impacts [26–29].

The asymmetric duration between El Niño and La Niña is influenced by various processes, including a nonlinear atmospheric response to SST [21,30], a contrasting effect of the Indian Ocean during the decay phase of El Niño and La Niña [31], and an asymmetric impact from the positive and negative phases of north Pacific meridional mode [32]. Additionally, a large heat discharge as well as delayed tropical inter-basin adjustment after strong El Niño events favors La Niña persistence [23]. Nonlinear oceanic dynamics also contribute; thermocline-driven SST anomalies are less effective at terminating La Niña [33], and cold SST from a previous La Niña event interrupts the heat recharge, facilitating a second-year La Niña [34]. Overall, the equatorial Pacific heat recharge associated with La Niña is weaker and less effective than the discharge related to El Niño [35], such that a La Niña decays slower and the cold SST anomalies persist longer.

Understanding and predicting ENSO phase transition have been a longstanding challenge. For example, prediction of the 2020–2022 La Niña itself carried a large uncertainty [36,37], not to mention the challenge of predicting the associated impact. After the event, suggestions were ripe that the three-year heat recharge of the 2020–2022 La Niña could precondition an extreme El Niño [38]. However, none of the extreme El Niño since 1950 follows a multiyear La Niña. Whether a multiyear La Niña favors a transition to an extreme El Niño is unknown, nor is how such a transition might be affected by greenhouse warming. Using observations and outputs from the sixth phase of the Coupled Model Intercomparison Project (CMIP6) [39], here we show that a transition from a multiyear La Niña to a strong or an extreme El Niño rarely occurs but is projected to be less rare under transient greenhouse warming.

2. Materials and methods

2.1. Observed and CMIP6 data

The SST data used here are averaged from three products, including Hadley Centre Sea Ice and SST dataset version 1.1 (HadISST v1.1) [40], Extended Reconstructed Sea Surface Temperature version 5 (ERSSTv5) [41], and Centennial in situ Observation-Based Estimates of Sea Surface Temperature version 2 (COBE-SST2) [42]. Outgoing longwave radiation (OLR) data used here are averaged from the fifth generation European Centre for Medium-Range Weather Forecasts (ECMWF) atmospheric reanalysis of the global climate (ERA5) [43] and the NOAA interpolated OLR product [44]. Sea surface height (SSH), heat content of upper 300 m and depth of 20 °C isotherm data are from the ECMWF Ocean Reanalysis System 5 (ORAS5) [45] and the wind stress data are from ERA5. We analyze datasets over the period of January 1958 to March 2024, and obtain monthly anomalies of the variables by removing climatological seasonal cycles of 1960–2022 period (1980–2022 period for NOAA interpolated OLR) and quadratic trends in each dataset.

We examine monthly outputs over the 1900–2099 period from 42 CMIP6 models forced by historical forcing up to 2014 and thereafter future greenhouse-gas forcing under a Shared Socioeconomic Pathway 5–8.5 (SSP585) scenario (Table S1 online) [39]. Changes in transition of a multiyear La Niña to an El Niño are compared between the 1900–1999 and the 2000–2099 period. Monthly anomalies of modelling outputs are obtained with reference to the monthly climatology of 1900–1999 and quadratically detrended on the basis of the full 200-year period (1900–2099) [4,12,28]. To test the sensitivity of our results, available models under different greenhouse-gas emission scenarios (SSP126, SSP245 and SSP370; Table S1 online) are also analyzed. All the observational and modelling data are interpolated to a $1^\circ \times 1^\circ$ grid.

2.2. Definition of ENSO events

In both observation and CMIP6 model outputs, we use 0.5 standard deviation (s.d.) of Niño3.4 index (i.e., SST anomalies in 5°S–5°N, 170°W–120°W) averaged over October to February (ONDJF) to define ENSO events, similar to ref. [28]. The s.d. is computed based on the Niño3.4 index over the 1958–2022 period of observation and 1900–1999 period of each CMIP6 model. A multiyear La Niña is identified as when the La Niña persists for two consecutive ONDJF seasons or more. We further use 1.5 s.d. and 2.0 s.d. of ONDJF Niño3.4 index to classify El Niño into moderate (0.5 s.d. $\leq$ Niño3.4 < 1.5 s.d.), strong (1.5 s.d. $\leq$ Niño3.4 < 2.0 s.d.) and extreme (Niño3.4 $\geq$ 2.0 s.d.) events. In observation, seven multiyear La Niña (Fig. 1a), seventeen moderate El Niño (**1963/1964**, 1965/1966, **1968/1969**, **1969/1970**, 1976/1977, **1977/1978**, **1986/1987**, **1987/1988**, **1991/1992**, **1994/1995**, **2002/2003**, **2004/2005**, 2006/2007, 2009/2010, **2014/2015**, 2018/2019, **2019/2020**), one strong El Niño (1972/1973) and three extreme El Niño (**1982/1983**, **1997/1998**, **2015/2016**) events are identified, which are generally consistent with previous studies using various methods to define ENSO amplitude and multiyear La Niña [4,23,28,29,46,47].

For a clear comparison, in our analyses of observation and CMIP6 outputs, only moderate, strong and extreme El Niño events that do not transition from a La Niña or a multiyear La Niña are included in the 'moderate El Niño', 'strong El Niño' and 'extreme El Niño' category (the events included in the observational analysis are labelled in bold), respectively. Only multiyear La Niña events that transition to an El Niño are included in the 'multiyear La Niña' category (in observation, these events are 1970–1971, 1973–1975, 2007–2008 and 2020–2022). Thus, there is no 'strong El Niño' category in the observational analysis because the only strong event, the 1972/1973 strong El Niño, follows 1970–1971 multiyear La Niña and is classified into the 'multiyear La Niña' category. We combine the 'strong El Niño' and 'extreme El Niño' categories in the analysis of CMIP6 outputs, because the two types of events have little distinct differences in the multievent-mean anomalous pattern or evolution of SSH, SST, surface wind, and convection during the period of February to June (FMAMJ).

2.3. Metrics of tropical deep convection

OLR is frequently used as a proxy for tropical atmosphere deep convection [6–11]. We use two metrics based on OLR to measure the activity of deep convection, which is nonlinearly correlated with local SST in the current and in a warmer climate [48]. Intensity of convection is measured by the OLR anomalies averaged over the equatorial central-eastern Pacific (5°S–5°N, 180°–100°W) (Fig. S1a, b online, black rectangle). A negative value of intensity indicates an enhanced deep convection. A location of convection center is measured by the longitude where the minimum total meridional mean (10°S–10°N, 120°E–90°W) of the OLR is located (Fig. S1c, d online, black dots). A negative (positive) location anomaly indicates a westward (eastward) movement of deep convection. There is a statistically significant negative correlation between the intensity and location of convection, as an eastward movement of convection enhances convection over the equatorial central-eastern Pacific. We apply a 3-month running mean to the

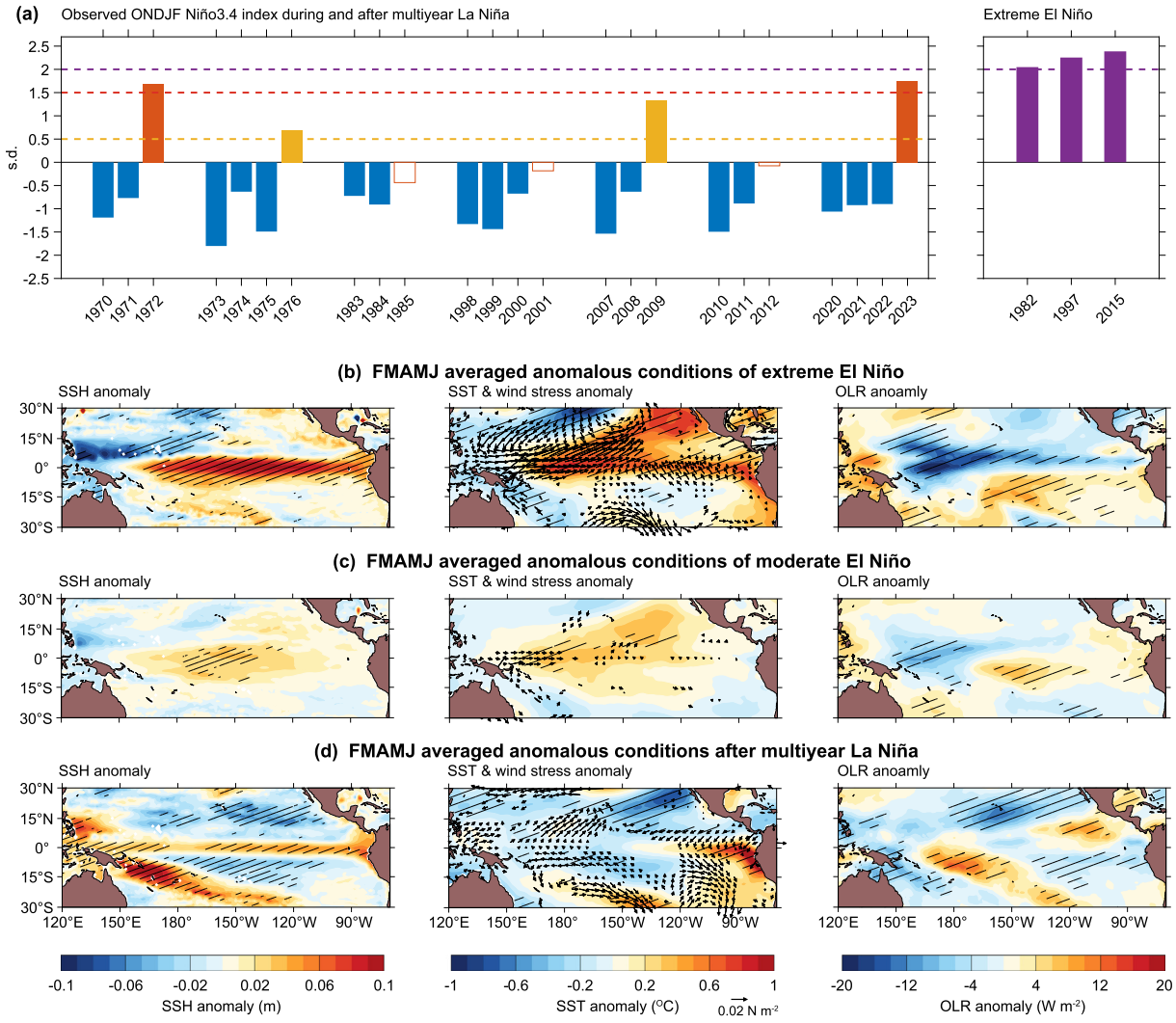

Fig. 1. Observed rare transition from a multiyear La Niña to a strong El Niño. (a) Normalized ONDJF averaged Niño3.4 SST index in the year during (blue bars) and after a multiyear La Niña, and of extreme El Niño (purple bars). Yellow, orange and purple dashed lines indicate threshold of identifying El Niño (0.5 s.d.), strong El Niño (1.5 s.d.) and extreme El Niño (2.0 s.d.), respectively. Orange and yellow bars indicate respective strong and moderate El Niño events, and hollow bars indicate neutral events. (b) Composite maps of FMAMJ averaged anomalous sea surface height (SSH; m) (left), SST (°C; colouring) and surface wind stress (N m^{-2}; vectors) (middle) and outgoing longwave radiation (OLR; W m^{-2}) (right) in the developing year of extreme El Niño events. (c) Same as (b) but for moderate El Niño events. (d) Same as (b) but for the year after multiyear La Niña. Values of multi-event mean exceeding 1.0 s.d. of the events are hatched (SSH, SST and OLR anomalies) or shown (surface wind stress). The events included in the composite are listed in '2.2 Definition of ENSO events' of Materials and methods. Due to a decoupled ocean and atmosphere over the tropical central and eastern Pacific during FMAMJ, a multiyear La Niña may transition to an El Niño in the subsequent winter, but rarely to a strong El Niño, and none to an extreme El Niño in the observation.

monthly anomalies of convection intensity, convection center location and central Pacific SST.

2.4. Bootstrap test

As in previous studies [4,12,28,47], we use a bootstrap resampling method [49] to examine whether the multimodel mean increase in the occurrence of multiyear La Niña transitioning to El Niño is statistically significant. The 21 occurrence numbers under historical forcing are resampled randomly to construct 10,000 realizations of mean occurrence number over 21 models, in which any occurrence number can be selected again. The same is carried out for the future period. The s.d. of the 10,000 inter-realizations of mean occurrence number for the two periods is computed, and we consider the increased mean occurrence number in 2000–2099 to be statistically significant above the 95% confidence level if the increased mean is greater than the sum of these two s.d. values. We also use the bootstrap test to examine the transition of multiyear La Niña to El Niño under other emission scenarios.

3. Results

3.1. Observed rare transition to strong El Niño

We use a 0.5 s.d. value of Niño3.4 SST index averaged over ONDJF as a threshold to define ENSO events, and a multiyear La Niña event involves at least two consecutive La Niña [28]. El Niño events are classified into moderate (0.5 s.d. $\leq$ Niño3.4 < 1.5 s.d.), strong (1.5 s.d. $\leq$ Niño3.4 < 2.0 s.d.), and extreme (Niño3.4 $\geq$ 2.0 s.d.) events using the magnitude of ONDJF Niño3.4 index (see '2.2 Definition of ENSO events' in Materials and methods). Seven multiyear La Niña events are identified from 1958 to 2023 (Fig. 1a), consistent with previous studies [23,24,28,29,46]. Four (Fig. 1a, orange and yellow bars) of the seven multiyear La Niña events transitioned to El Niño events, of which only two were

strong (Fig. 1a, orange bar) and none was extreme. The remaining three multiyear La Niña events transitioned to a neutral state (Fig. 1a, hollow bars).

Collectively, the statistics indicate that a multiyear La Niña may transition to an El Niño in the subsequent winter, but rarely to a strong El Niño, even less so to an extreme El Niño. This is somewhat unexpected, as the recharged equatorial western Pacific heat content tends to be greater after a multiyear La Niña [38] than that preceding a moderate or even an extreme El Niño (Fig. S2 online). A changing background condition might have an impact [50] but whether it is related to greenhouse warming is not clear.

3.2. Decoupled ocean and atmosphere after a multiyear La Niña

The slower growth of warm SST anomalies after a multiyear La Niña compared with those during moderate and extreme El Niño events results from a decoupled ocean and atmosphere over the period of FMAMJ, the early developing stage of a typical El Niño. During FMAMJ of an extreme El Niño event, anomalous thermocline deepening in the equatorial central-eastern Pacific (Fig. 1b, left; Fig. S3a, d online) and anomalous westerly winds over the equatorial western-central Pacific (Fig. 1b, middle) induce a warm SST anomaly, involving thermocline feedback, zonal advective feedback and Ekman pumping feedback [51,52]. In association, atmosphere deep convection, as measured by negative OLR anomalies, enhances over the eastern edge of warm pool and extends to the eastern Pacific (Fig. 1b, right), further increasing the anomalous westerlies that push the warm water and deep convection eastward (Fig. S3a online). The warm SST and westerly wind anomalies reinforce each other under the Bjerknes feedback with a strong ocean-atmosphere coupling, facilitating a rapid growth of warm SST anomalies. An extreme El Niño requires an eastward displaced warm pool edge in addition to a recharged ocean heat content [53].

During a moderate El Niño, anomalies of thermocline depth (Fig. 1c, left; Fig. S3b, e online), surface wind and SST (Fig. 1c, middle) are weaker and more concentrated in the central Pacific compared to those during an extreme El Niño, resembling characteristics of a central-Pacific type El Niño [54]. The category of moderate El Niño involves many events that are usually identified as central-Pacific El Niño (see '2.2 Definition of ENSO events' in Materials and methods). Although relatively weak, the deep convection enhances and moves eastward (Fig. 1c, right), indicating an active ocean-atmosphere coupling.

In a sharp contrast, during FMAMJ after a multiyear La Niña, the thermocline deepens along the equator within a narrow meridional band (2°S–2°N) in response to Kelvin waves, accompanied by an anomalously shallow thermocline in broad regions both sides of the equator (Fig. 1d, left; Fig. S3c, f online). The SST remains anomalously cold in the equatorial Pacific except in a small area of the far-eastern Pacific, and easterly wind anomalies prevail in the equatorial western-central Pacific (Fig. 1d, middle). The deep convection is confined to the warm pool because of the central Pacific cold conditions (Fig. 1d, right), leading to a decoupled ocean and atmosphere that delay the growth of warm SST anomalies.

We use two OLR-based metrics including a location of convection center and an intensity of convection to further examine the activity of atmosphere deep convection (see '2.3 Metrics of tropical deep convection' in Materials and methods and Fig. S1 online). The convection center is defined as the longitude where the minimum total meridional mean (10°–10°N) of the OLR is located, and the intensity is defined as OLR anomalies averaged over the equatorial central-eastern Pacific (5°S–5°N, 180°–100°W), both of which are closely related to the central Pacific warming [9,10,55]. The convection center is sensitive to the central Pacific SST anomaly and moves to the east (positive anomaly) during FMAMJ of a moderate or an extreme El Niño, underpinned by a statistically significant regression slope (Fig. 2a, yellow and red dots).

In comparison, the convection center remains within the western Pacific (a negative location anomaly) during FMAMJ after a multiyear La Niña, with negative central Pacific SST anomalies inhibiting the eastward migration of deep convection (Fig. 2a, blue dots). Consistent with an eastward movement of the convection center, the intensity of convection enhances over the central-eastern Pacific in response to an increased central Pacific SST anomaly in a moderate or an extreme El Niño (Fig. S4a online, yellow and red dots). By contrast, the response is much weaker after a multiyear La Niña (Fig. S4a online, blue dots), as indicated by a smaller slope.

The contrast in deep convection activity is also manifested in a monthly evolution. During an extreme El Niño, a central Pacific warming emerges early, activating a response of deep convection, hence an onset of ocean-atmosphere coupling (Fig. 2b and Fig. S4b online, red arrows). The Bjerknes positive feedback operates in the ensuring months, producing extreme SST and convection anomalies in boreal winter. The central Pacific SST increases approximately by 1.8 °C by December, associated with an approximately 50°-longitude eastward movement and approximately 40 W m^{-2} enhancement of atmosphere convection. During a moderate El Niño, there is a weak central Pacific warming but active ocean-atmosphere coupling (Fig. 2b and Fig. S4b online, yellow arrows), consistent with the composites (Fig. 1c). The intensity of central Pacific warm anomalies, eastward movement, and enhancement of convection, are approximately 1/2, 1/3, and 1/8, respectively, of that associated with an extreme El Niño.

After a multiyear La Niña, however, the equatorial cold conditions persist until June, before which time establishment of deep convection over the central Pacific does not occur (Fig. 2b and Fig. S4b online, blue arrows). Growth of SST anomalies is curtailed in the absence of an active ocean-atmosphere coupling, unfavorable to preconditioning a strong or an extreme El Niño in the ensuring months. The persistent cold SST anomalies in the central equatorial Pacific prior to June reflect the slow-decay characteristic of La Niña [21,23,30–35].

3.3. Rare but more frequent future transition to strong El Niño

Considering that multiyear La Niña and its transition is a part of ENSO asymmetry, we examine the ability of CMIP6 models to reproduce the observed ENSO asymmetry in historical simulations over the 1900–1999 period. The asymmetry of a longer persistence but a weaker amplitude of La Niña compared with El Niño is manifested in a positive skewness of SST anomalies in the central-eastern equatorial Pacific (i.e., Niño3.4 region). A total of 21 out of 42 models simulate a positive Niño3.4 skewness (Fig. S5 online, red bars), and these 21 models are selected for further analysis as in a previous study [28]. Models with a positive Niño3.4 skewness simulate reasonably well the observed nonlinear ENSO dynamics and multiyear La Niña properties [28,47].

The selected models reproduce the observed contrasting development during FMAMJ of different El Niño events in the historical simulations. For example, the anomalous deepening thermocline, warm SST and westerlies grow fast under a strong ocean-atmosphere coupling during an extreme or a strong El Niño, associated with enhanced and eastward extended deep convection (Fig. 3a and Fig. 1b). Here, we combine the extreme and strong El Niño events in the modelling analyses as there are no distinct differences in their early-developing features especially in the deep convection activities. During a moderate El Niño, ocean-atmosphere coupling is active though weaker, and the growth of El Niño anomalies is similar to that of an extreme or a strong El Niño (Fig. 3b and Fig. 1c). By FMAMJ after a multiyear La Niña,

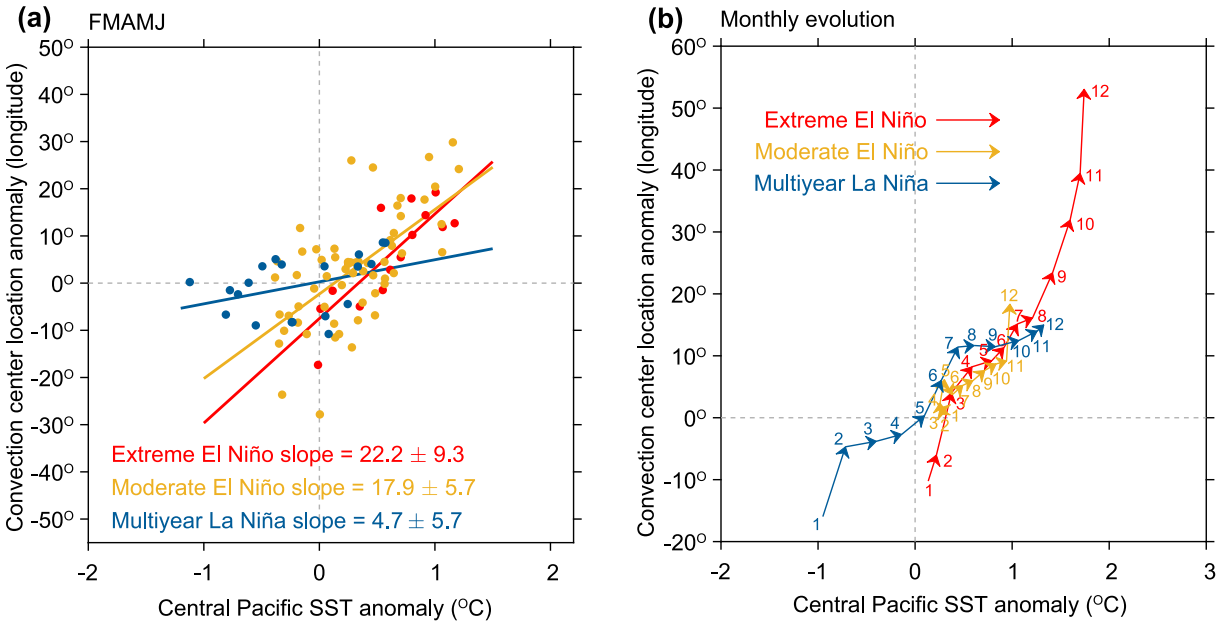

Fig. 2. Decoupled ocean and atmosphere during an early developing stage of El Niño after a multiyear La Niña. (a) Relationship between anomalous location of convection center and central Pacific SST anomalies (averaged in 5°S–5°N, 180°–140°W) during FMAMJ of an extreme El Niño (red dots), a moderate El Niño (yellow dots) and after a multiyear La Niña (blue dots). Each dot represents a calendar month of FMAMJ. Also shown are respective slopes with 95% confidence intervals. The contrast in slopes between that after multiyear La Niña and that of moderate and extreme El Niño is statistically significantly above the 95% confidence level based on a *t*-test. (b) Monthly evolution of relationship between anomalous location of convection center and central Pacific SST anomalies in multievent mean of extreme El Niño (red arrow and number), moderate El Niño (yellow) and after multiyear La Niña (blue). The numbers indicate respective calendar months. The ENSO events analyzed here are listed in '2.2 Definition of ENSO events' of Materials and methods. The location and intensity of convection are measured by OLR (see '2.3 Metrics of tropical deep convection' in Materials and methods). The persistent cold conditions in boreal spring and early summer after multiyear La Niña inhibit an eastward movement and enhancement of atmosphere deep convection, leading to a decoupled ocean and atmosphere that delay the growth of subsequent El Niño.

however, warm SST and westerly wind anomalies have not developed in the equatorial western-central Pacific due to a decoupled ocean and atmosphere (Fig. 3c and Fig. 1d).

We compute the occurrence of transition from a multiyear La Niña to an El Niño over the 1900–1999 period in each of the selected models, and compare with that over the 2000–2099 period, using outputs from simulations under a future high-emission warming scenario (SSP585) [39]. A total of 16 of the 21 selected models (76.2%) simulate an increase in such transition under future climate, with another two models (MRI-ESM2-0 and UKESM1-0-LL) simulating unchanged occurrences (Fig. 3d). The multimodel mean increase is at 101.9% ± 31.4%. The frequency of transition from a multiyear La Niña to a strong or an extreme El Niño increases, but is likewise rare. The multimodel total occurrences increase from 13 to 33 cases in the aggregated 2100 years in terms of a multiyear La Niña transition to a strong or an extreme El Niño, and from 4 to 18 cases in the aggregated 2100 years in terms of a multiyear La Niña transition to an extreme El Niño. These multimodel mean increases are statistically significant above the 95% confidence level (Fig. 3d, 'MME-all', 'MME-strong & extreme', 'MME-extreme'), according to a Bootstrap method (see '2.4 Bootstrap test' in Materials and methods).

The transition of a multiyear La Niña to an El Niño in the twentieth century (1900–1999) is underestimated by the models, compared with approximately one case every 16.5 years (4 cases in 66 years) in the observation (Fig. 1a). The underestimation may result from a long-standing model bias of a too-cold and too-far-west Pacific cold tongue [4,56,57], which makes the establishment and eastward movement of deep convection over the central-eastern Pacific even more difficult after a multiyear La Niña, hence a lower probability of transition to an El Niño. The increased frequency in the transition from a multiyear La Niña to an El Niño occurs in other emission scenarios (Fig. 3d, right of the vertical line), with a multimodel mean increase of 68.6% ± 29.8%, 96.3% ± 37.4% and 86.1% ± 31.2%, respectively, under SSP126, SSP245 and SSP370, statistically significant above the 95% confidence level according to a bootstrap test (Fig. S6 online). Given that ENSO's response to greenhouse warming is nonlinear and substantially modulated by the tropical Pacific mean warming pattern [58], the extent to which the transition of multiyear La Niña responds to varying amplitudes of greenhouse-gas forcing remains an open question.

3.4. Projected mean state change facilitates a transition

In the twenty-first century, during FMAMJ after a multiyear La Niña, the ocean and atmosphere continue to be unfavorable to ocean-atmosphere coupling (Fig. S7 online), a condition that determines the rare occurrence of a subsequent strong or extreme El Niño. The increased likelihood of transition from a multiyear La Niña to an El Niño under global warming results from a stronger convection sensitivity to SST anomalies in general [4,12,59,60]. The higher sensitivity of atmosphere convection intensity to an anomalous central Pacific SST anomaly during FMAMJ after a multiyear La Niña (Fig. 4a, b, blue dots) is illustrated by a statistically significant larger regression slope in 2000–2099 than that in 1900–1999, similar to the increased sensitivity during a moderate El Niño (Fig. 4a, b, yellow dots), but less so during an extreme El Niño (Fig. 4a, b, red dots), in which the anomalous convection is already intense over the historical period. Using location of the convection center to represent the convection activity yields a similar result (Fig. S8a, b online).

For each selected model, we apply a regression of monthly anomalous convection intensity onto time series of averaged cen-

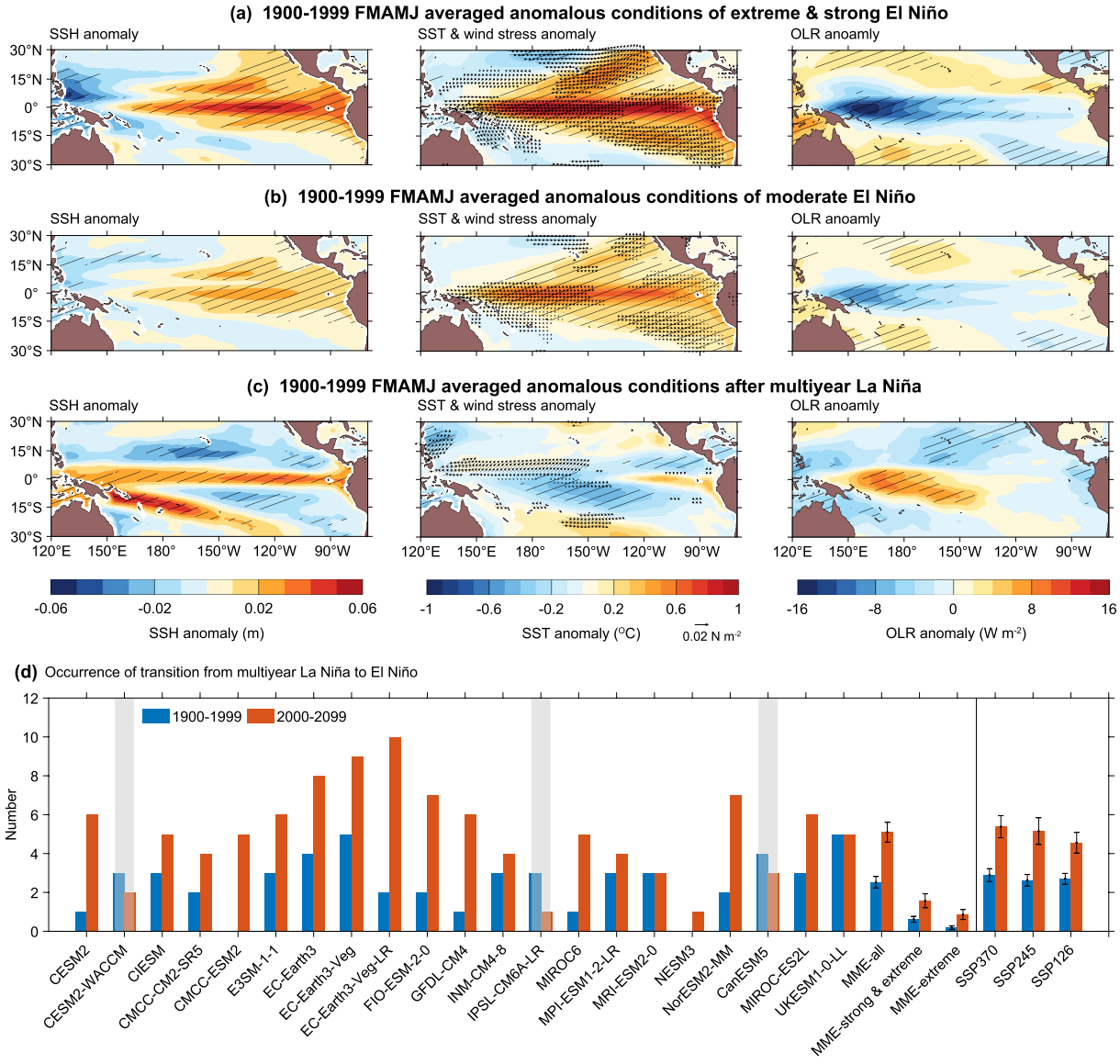

Fig. 3. Rare but more likely transitions from a multiyear La Niña to a strong El Niño under greenhouse warming. (a–c), Same as Fig. 1 b–d but for FMAMJ of (a) strong and extreme El Niño events, (b) moderate El Niño events and (c) after multiyear La Niña over 1900–1999 in the selected models. The mean values that exceed 1.0 s.d. are hatched (SSH, SST and OLR anomalies) or shown (surface wind stress). CESM2 is not involved in the OLR composite owing to data unavailability. (d) Comparison of the number of El Niño events transitioning from a multiyear La Niña over 1900–1999 (blue bars) and 2000–2099 (red bars) in the selected models under historical and SSP585 scenario (left of the vertical line). Models that simulate a decrease are greyed out. The multimodel ensemble mean (MME) numbers of all El Niño events (Niño3.4 $\geq$ 0.5 s.d.), strong and extreme El Niño events (Niño3.4 $\geq$ 1.5 s.d.) and extreme El Niño events (Niño3.4 $\geq$ 2.0 s.d.) transitioning from a multiyear La Niña are labeled as 'MME-all', 'MME-strong & extreme' and 'MME-extreme', respectively. MME results under other emission scenarios (right to the vertical line) are provided using the selected ensembles (Table S1 online). Error bars on the multimodel mean are calculated as 1.0 s.d. of 10,000 inter-realizations of a bootstrap method (see '2.4 Bootstrap test' in Materials and methods). Selected models reproduce the observed ocean-atmosphere decoupling after a multiyear La Niña, and simulate an increase in the transition from a multiyear La Niña to an El Niño under greenhouse warming, although still rare.

tral Pacific SST anomalies over their FMAMJ values of every year, separately over the 1900–1999 and 2000–2099 period (500 values in each period), and multiply the regression coefficients by the respective s.d. of the anomalous central Pacific SST anomalies to obtain a total response. In the future climate, a stronger response (more negative) is seen in most models (Fig. 4c), and models that simulate a larger enhancement in the response systematically produce more occurrences of transition from a multiyear La Niña to an El Niño, with a statistically significant inter-model correlation (r = –0.56, P = 0.0107). The stronger convection response is facilitated by a projected mean state change, as indicated by an inter-model correlation between changes in the total response and in the mean SST pattern (Fig. 4d).

Under greenhouse warming, a western Pacific warm pool expansion and a diminished climatological zonal SST gradient induced by a faster warming in the equatorial eastern Pacific than in the western promotes establishment and its eastward shift of atmosphere deep convection [4,12,59,60]. Further, the upper-ocean stratification of the equatorial Pacific increases as the surface ocean warms faster than the ocean below, leading to an enhanced ocean-atmosphere coupling such that the SST anomalies are more sensitive to a given wind forcing [2,47]. Both are conducive to an onset of ocean-atmosphere coupling, hence to occurrences of El Niño transitioned from all preconditions, including multiyear La Niña condition. Results using the total response of convection movement to the central Pacific SST anomalies further highlight the crucial role of the mean state warming pattern and the associated stronger convection response in the more frequent transition from a multiyear La Niña to an El Niño. The enhanced (a higher positive value) response is significantly positively correlated

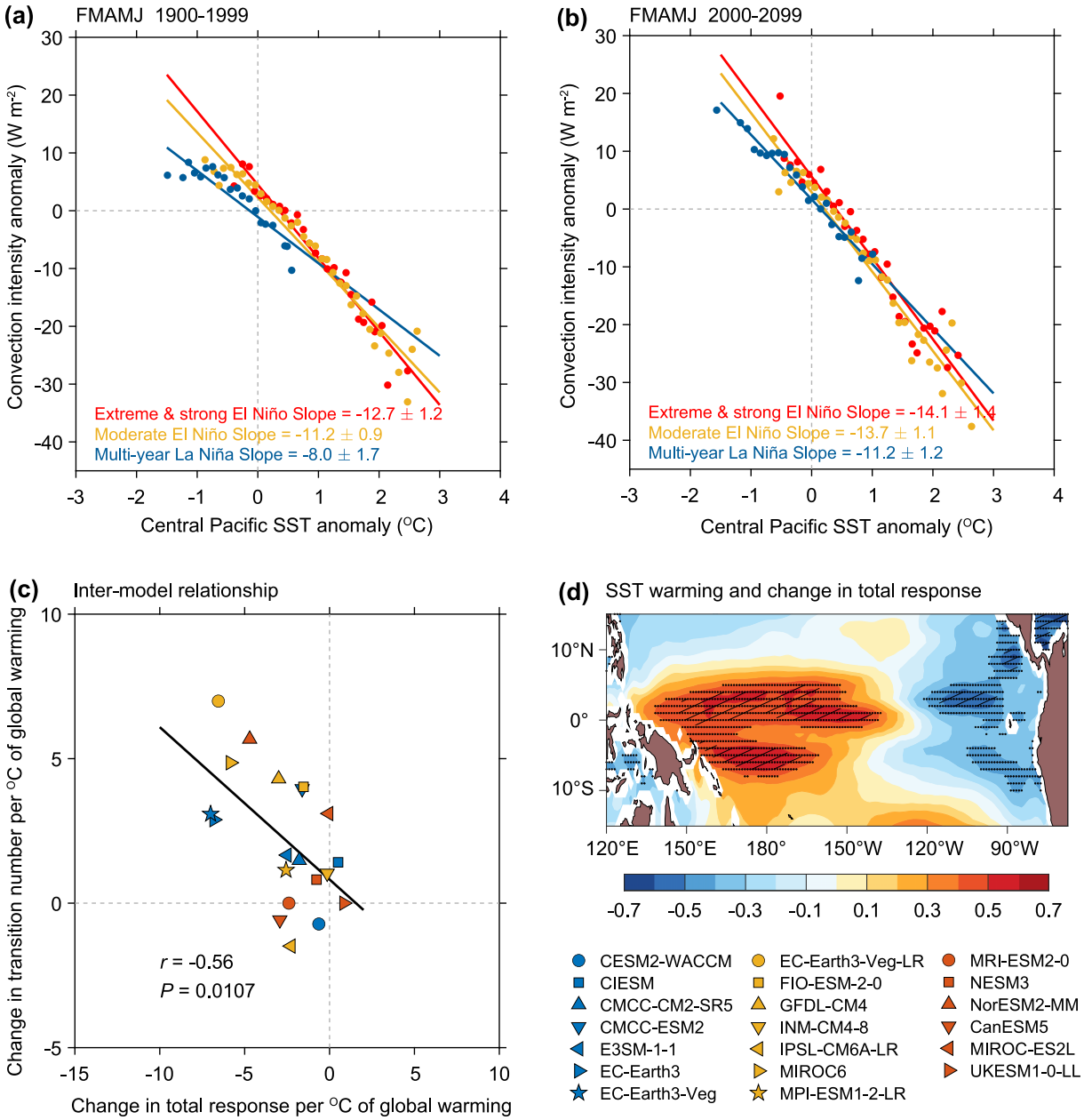

Fig. 4. Mean state changes facilitate a transition from a multiyear La Niña to a strong El Niño. (a) Relationship of anomalous convection intensity with central Pacific SST anomalies (averaged in 5°S–5°N, 180°–140°W) during FMAMJ of strong and extreme El Niño (red dots), moderate El Niño only (yellow dots) and after multiyear La Niña (blue dots) over the 1900–1999 period. The convection intensity anomalies are binned in 0.1 °C central Pacific SST anomaly intervals to obtain median anomaly in each bin. Also shown are respective slopes with 95% confidence intervals. (b) Same as (a) but for results over the 2000–2099 period. (c) Inter-model relationship between the change (2000–2099 minus 1900–1999) in El Niño numbers transitioning from a multiyear La Niña and the change in the total response (W m^{-2}) of convection intensity to central Pacific SST anomalies. Changes in each model are scaled by the corresponding increase in global mean SST. Linear fit is displayed together with correlation coefficient *r* and *P* value. (d) Inter-model correlation between changes (2000–2099 minus 1900–1999) in grid-point mean SST with changes in the total response of convection intensity to central Pacific SST anomalies, both scaled by the increase in global mean SST of each model. Stippling (hatching) indicates statistical significance above the 90% (95%) level based on a two-tailed Student's *t*-test. CESM2 is not involved here owing to data unavailability. Under greenhouse warming, the projected mean state change promotes ocean-atmosphere coupling, facilitating the transition from a multiyear La Niña to a strong or an extreme El Niño.

(r = 0.55, P = 0.012) with the increased transition frequency (Fig. S8c online), and is linked to the mean SST warming (Fig. S8d online).

4. Discussion and conclusion

We find that a multiyear La Niña rarely transitions to a strong or an extreme El Niño, despite a multiyear-long heat recharge of the equatorial Pacific. The rarity is underpinned by the cold SST anomalies in the central equatorial Pacific and an anomalously shallow thermocline in the equatorial Pacific that persist into early boreal summer, even after the multiyear La Niña recharge. These cold conditions are in turn associated with the slow recharge and nonlinear dynamics that contribute to the slow decay of La Niña [21,23,30–35]. The persistent anomalies anchor the atmosphere deep convection and heavy rainfall over the western Pacific warm pool region. Consequently, the anomalous atmosphere deep convection is unable to move eastward, and the ocean and atmosphere are decoupled over the equatorial central Pacific in the early developing stage of El Niño, delaying and limiting the subsequent growth of warm anomalies. Under future greenhouse warming, a

faster warming in the equatorial eastern Pacific than the surrounding regions facilitates an eastward movement of atmosphere deep convection [4,12,59,60], and an intensified upper ocean stratification enhances ocean-atmosphere coupling [2,47]. These changes ensure that an eastward movement of deep convection is more sensitive to warm SST anomalies and an onset of ocean-atmosphere coupling in the central equatorial Pacific is more readily triggered, increasing the transition from a multiyear La Niña to a strong or an extreme El Niño. Our result contributes to our understanding and prediction of ENSO transition, and suggests that swings from a multiyear La Niña to a strong El Niño, though still rare, are more likely in the twenty-first century.

Conflict of interest

The authors declare that they have no conflict of interest.

Acknowledgments

This work is supported by the National Key Research and Development Program of China (2020YFA0608801), National Natural Science Foundation of China (42376006), China's National Key Research and Development Projects (2023YFF0805200) and the Science and Technology Innovation Project of Laoshan Laboratory (LSKJ202203300). Fan Jia is supported by Laoshan Laboratory (LSKJ202202402), and Taishan Scholars Program (tsqn202312265). Tao Geng is supported by NSFC project (42206209, and 42276006) and China National Postdoctral Program for Innovative Talents (BX20220279). We acknowledge the World Climate Research Programme, which, through its Working Group on Coupled Modelling, coordinated and promoted CMIP6. We thank the climate modelling groups for producing and making available their model output, the Earth System Grid Federation (ESGF) for archiving the data and providing access and the multiple funding agencies who support CMIP6 and ESGF. Pacific Marine Environmental Laboratory (PMEL) contribution number 5585.

Author contributions

Fan Jia, Wenju Cai and Tao Geng designed the study and wrote the initial manuscript in discussion with Lixin Wu. Fan Jia performed analysis and generated all figures with Tao Geng. All authors contributed to interpreting the results and improving the paper.

Data availability

Data related to the paper can be downloaded from the following websites:

HadISST v1.1, https://www.metoffice.gov.uk/hadobs/hadisst/;

ERSST v5, https://psl.noaa.gov/data/gridded/data.noaa.ersst.v5.html;

COBE-SST2, https://psl.noaa.gov/data/gridded/data.cobe2.html;

ERA5, https://www.ecmwf.int/en/forecasts/dataset/ecmwf-reanalysis-v5;

ORAS5, https://www.ecmwf.int/en/research/climate-reanalysis/ocean-reanalysis;

NOAA interpolated OLR, https://psl.noaa.gov/data/gridded/data.olrcdr.interp.html;

CMIP6, https://esgf-node.llnl.gov/projects/cmip6/.

All codes are available from the corresponding author(s) on request.

Appendix A. Supplementary material

Supplementary data to this article can be found online at https://doi.org/10.1016/j.scib.2024.12.034.

References

[1] McPhaden MJ, Zebiak SE, Glantz MH. ENSO as an integrating concept in earth science. Science 2006;314:1740–2175.
[2] Collins M, An SI, Cai W, et al. The impact of global warming on the tropical Pacific Ocean and El Niño. Nat Geosci 2010;3:391–7.
[3] Yeh SW, Cai W, Min SK, et al. ENSO atmospheric teleconnections and their response to greenhouse gas forcing. Rev Geophys 2018;56:185–206.
[4] Cai W, Santoso A, Collins M, et al. Changing El Niño–Southern Oscillation in a warming climate. Nat Rev Earth Environ 2021;2:628–44.
[5] Bjerknes J. Atmospheric teleconnections from the equatorial Pacific. Mon Weath Rev 1969;97:163–72.
[6] Chiodi AM, Harrison DE. Characterizing warm ENSO variability in the equatorial Pacific: An OLR perspective. J Clim 2010;23:2428–39.
[7] Chiodi AM, Harrison DE. El Niño impacts on seasonal U.S. atmospheric circulation, temperature, and precipitation anomalies: the OLR-event perspective. J Clim 2013;26:822–37.
[8] Chiodi AM, Harrison DE. Global seasonal precipitation anomalies robustly associated with El Niño and La Niña events—An OLR perspective. J Clim 2015;28:6133–59.
[9] Johnson NC, L'Heureux ML, Chang CH, et al. On the delayed coupling between ocean and atmosphere in recent weak El Niño episodes. Geophys Res Lett 2019;46:11416–25.
[10] Johnson NC, Kosaka Y. The impact of eastern equatorial Pacific convection on the diversity of boreal winter El Niño teleconnection patterns. Clim Dyn 2016;47:3737–65.
[11] L'Heureux ML, Tippett MK, Barnston AG. Characterizing ENSO coupled variability and its impact on North American seasonal precipitation and temperature. J Clim 2015;28:4231–45.
[12] Cai W, Borlace S, Lengaigne M, et al. Increasing frequency of extreme El Niño events due to greenhouse warming. Nat Clim Chang 2014;4:111–6.
[13] Takahashi K, Dewitte B. Strong and moderate nonlinear El Niño regimes. Clim Dyn 2016;46:1627–45.
[14] Jin FF. An equatorial ocean recharge paradigm for ENSO. Part I: conceptual model. J Atmos Sci 1997;54:811–29.
[15] Vecchi GA. The termination of the 1997/98 El Niño. Part II: mechanisms of atmospheric change. J Clim 2006;19:2647–64.
[16] McGregor S, Timmermann A, Schneider N, et al. The effect of the South Pacific convergence zone on the termination of El Niño events and the meridional asymmetry of ENSO. J Clim 2012;25:5566–86.
[17] Kessler WS. Is ENSO a cycle or a series of events? Geophys Res Lett 2002;29:401–4.
[18] An SI, Jin FF. Nonlinearity and asymmetry of ENSO. J Clim 2004;17:2399–412.
[19] Capotondi A, Wittenberg AT, Newman M, et al. Understanding ENSO diversity. Bull Am Meteorol Soc 2015;96:921–38.
[20] Timmermann A, An SI, Kug JS, et al. El Niño–Southern Oscillation complexity. Nature 2018;559:535–45.
[21] Okumura YM, Deser C. Asymmetry in the duration of El Niño and La Niña. J Clim 2010;23:5826–43.
[22] DiNezio PN, Deser C, Okumura YM, et al. Predictability of 2-year La Niña events in a coupled general circulation model. Clim Dyn 2017;49:4237–61.
[23] Wu X, Okumura YM, DiNezio PN. What controls the duration of El Niño and La Niña events? J Clim 2019;32:5941–65.
[24] Park JH, An SI, Kug JS, et al. Mid-latitude leading double-dip La Niña. Int J Climatol 2021;41:E1353–70.
[25] Kim JW, Yu JY. Single- and multi-year ENSO events controlled by pantropical climate interactions. npj Clim Atmos Sci 2022;5:88.
[26] Wang J, Chen Y, Nie J, et al. On the role of anthropogenic warming and wetting in the July 2021 Henan record-shattering rainfall. Sci Bul 2022;67:2055–9.
[27] Lopes AB, Andreoli RV, Souza RAF, et al. Multiyear La Niña effects on the precipitation in South America. Int J Climatol 2022;42:9567–82.
[28] Geng T, Jia F, Cai W, et al. Increased occurrences of consecutive La Niña events under global warming. Nature 2023;619:774–81.
[29] Wang B, Sun W, Jin C, et al. Understanding the recent increase in multiyear La Niñas. Nat Clim Chang 2023;13:1075–81.
[30] Ohba M, Ueda H. Role of nonlinear atmospheric response to SST on the asymmetric transition process of ENSO. J Clim 2009;22:177–92.
[31] Okumura YM, Ohba M, Deser C, et al. A proposed mechanism for the asymmetric duration of El Niño and La Niña. J Clim 2011;24:3822–4389.
[32] Fan H, Wang C, Yang S. Asymmetry between positive and negative phases of the Pacific Meridional Mode: A contributor to ENSO transition complexity. Geophys Res Lett 2023;50:e2023GL104000.
[33] DiNezio PN, Deser C. Nonlinear controls on the persistence of La Niña. J Clim 2014;27:7335–55.
[34] Hu ZZ, Kumar A, Xue Y, et al. Why were some La Niñas followed by another La Niña? Clim Dyn 2014;42:1029–42.

[35] Li X, Hu ZZ, Zhao S, et al. On the asymmetry of the tropical Pacific thermocline fluctuation associated with ENSO recharge and discharge. Geophys Res Lett 2022;49:e2022GL099242.
[36] Zhang RH, Gao C, Feng L. Recent ENSO evolution and its real-time prediction challenges. Natl Sci Rev 2022;9:nwac052.
[37] Hasan NA, Chikamoto Y, McPhaden MJ. The influence of tropical basin interactions on the 2020-22 double-dip La Niña. Front Clim 2022;4:1001174.
[38] Lian T, Wang J, Chen D, et al. A Strong 2023/24 El Niño is Staged by Tropical Pacific Ocean Heat Content Buildup. Ocean-Land-Atmos Res 2023;2:0011.
[39] Eyring V, Bony S, Meehl GA, et al. Overview of the Coupled Model Intercomparison Project Phase 6 (CMIP6) experimental design and organization. Geosci Model Dev 2016;9:1937–58.
[40] Rayner NAA, Parker DE, Horton EB, et al. Global analyses of sea surface temperature, sea ice, and night marine air temperature since the late nineteenth century. J Geophys Res Atmos 2003;108:4407.
[41] Huang B, Thorne PW, Banzon VF, et al. Extended reconstructed sea surface temperature, version 5 (ERSSTv5): upgrades, validations, and intercomparisons. J Clim 2017;30:8179–205.
[42] Hirahara S, Ishii M, Fukuda Y. Centennial-scale sea surface temperature analysis and its uncertainty. J Clim 2014;27:57–75.
[43] Hersbach H, Bell B, Berrisford P, et al. ERA5 Monthly Averaged Data on Single Levels from 1959 To Present (Copernicus Climate Change Service Climate Data Store, 2019).
[44] Liebmann B, Smith CA. Description of a complete (interpolated) outgoing long wave radiation dataset. Bull Am Meteorol Soc 1996;77:1275–7.
[45] Zuo H, Balmaseda MA, Tietsche S, et al. The ECMWF operational ensemble reanalysis-analysis system for ocean and sea ice: a description of the system and assessment. Ocean Sci 2019;15:779–808.
[46] Kim JW, Yu JY, Tian B. Overemphasized role of preceding strong El Niño in generating multi-year La Niña events. Nat Commun 2023;14:6790.
[47] Cai W, Wang G, Dewitte B, et al. Increased variability of eastern Pacific El Niño under greenhouse warming. Nature 2018;564:201–6.
[48] Leung JCH, Zhang B, Gan Q, et al. Differential expansion speeds of Indo-Pacific warm pool and deep convection favoring pool under greenhouse warming. npj Clim Atmos Sci 2022;5:97.
[49] Austin PC, Tu JV. Bootstrap methods for developing predictive models. Am Stat 2004;58:131–7.
[50] Li X, Hu ZZ, McPhaden MJ, et al. Triple-dip La Niñas in 1998–2001 and 2020–2023: Impact of mean state changes. J Geophys Res Atmos 2023;128:e2023JD038843.
[51] An SI, Jin FF. Collective role of thermocline and zonal advective feedbacks in the ENSO mode. J Clim 2001;14:3421–32.
[52] Jin FF, Kim ST, Bejarano L. A coupled-stability index for ENSO. Geophys Res Lett 2006;33:L23708.
[53] Fu S, Hu S, Zheng XT. Collaborative role of warm pool edge and ocean heat content in El Niño development: implications for the 1982/83 extreme El Niño. Clim Dyn 2024;62:7701–16.
[54] Kug JS, Jin FF, An SI. Two types of El Niño events: cold tongue El Niño and warm pool El Niño. J Clim 2009;22:1499–515.
[55] Hu ZZ, McPhaden MJ, Kumar A, et al. Uncoupled El Niño warming. Geophys Res Lett 2020;47:e2020GL087621.
[56] Bayr T, Latif M, Dommenget D, et al. Mean-state dependence of ENSO atmospheric feedbacks in climate models. Clim Dyn 2018;50:3171–94.
[57] Planton YY, Guilyardi E, Wittenberg AT, et al. ENSO evaluation in climate models: the CLIVAR 2020 metrics package. Bull Am Meteorol Soc 2020;102:E193–217.
[58] Geng T, Cai W, Jia F, et al. Decreased ENSO post-2100 in response to formation of a permanent El Niño-like state under greenhouse warming. Nat Comm 2024;15:5810.
[59] Xie SP, Deser C, Vecchi GA, et al. Global warming pattern formation: sea surface temperature and rainfall. J Clim 2010;23:966–86.
[60] Power SB, Delage F, Chung C, et al. Robust twenty-first century projections of El Niño and related precipitation variability. Nature 2013;502:5415.